Improving Transparency of Powered Exoskeletons Using Force/Torque Sensors on the Supporting Cuffs

Damiano Zanotto *Member, IEEE*, Tommaso Lenzi *Member, IEEE*,
Paul Stegall *Student Member, IEEE* and Sunil K. Agrawal *Member, IEEE*

***Abstract*—Most of the control strategies embedded in recent robotic exoskeletons for rehabilitation and assistance are specific implementations of the well-known "assistance as needed" paradigm. A key point in the design of these systems is the requirement for the robot to exert negligible interaction forces to the wearer if he/she is performing well. Optimizing transparency of a device is a challenging task: various strategies have been proposed to achieve this goal, involving both the mechanical structure of the robot and the control algorithms. In this work, we propose a simple yet effective approach that requires minimal redesign efforts in the robotic structure and in the controller to be implemented on existing devices. We experimentally validate the method by comparing kinematic, kinetic and electromyographic data collected from 3 healthy subjects as they walked in three different conditions: free treadmill walking, walking in a robotic trainer with a traditional zero-impedance configuration and walking in the same robot with the new zero-impedance configuration. Results show that the novel configuration was capable of effectively reducing the interaction forces and, as a consequence, it affected subjects' natural gait less than the traditional one did.**

I. Introduction

Powered exoskeleton are used in motor rehabilitation to guide patient's movement during the rehabilitative tasks. Earlier versions of lower-limb exoskeletons for rehabilitation used a rigid position control to move the legs of the user along a specific trajectory. Research in the rehabilitation field later pointed out the need to promote the active participation of the patient, in order to maximize the rehabilitation outcome (assistance as needed paradigm [1]). Therefore, the robot should provide only the support that is needed for a correct execution of the movement, and should not interfere with the wearer when he/she performs the assigned task correctly. To this end, most exoskeleton controllers switched from the earlier rigid position control to more flexible torque controllers that allow the implementation of compliant force fields, or other more complex high-level strategies that adapt the support to the wearer based on his/her performance (slacking prevention). In order to be effective, a basic requirement for these controllers is *transparency*, i.e., the capability of the robot to have nil interaction with the user when no corrective force is being applied. From an engineering viewpoint this is a challenging task, since the mechanical impedance of the robot (i.e., the effects of its inertia, friction and weight) must be compensated by the controller. Most of the existing powered exoskeletons for gait rehabilitation are controlled by closing a feedback loop on single-axis sensors at the joint level [2], [3]. This closed loop controller can mask the inertia and friction of the actuator when disturbances are inside the closed-loop rejection bandwidth. Nevertheless, the dynamics of the robot links cannot be compensated by this force feedback control alone. Indeed, since the torques are measured at the level of the powered joints, the torque contributions required to move the robot links must be provided by the user. Available techniques for reducing this effect include inertial compensators based on feed-forward filters [4] or positive feedback [5]. However, these approaches require an on-line estimate of the acceleration, which is difficult to obtain without noise amplification or phase delays [4]. For this reason, feed-forward compensation is usually utilized for gravity and friction only, while advanced inertia compensation techniques are currently limited to single degree-of-freedom (DOF) devices. An alternative approach consists in minimizing the inertia of the robotic links by adopting parallel kinematic chains [6] or cable-driven designs [3], [4] to remotely actuate links. However, this often leads to complex and more expensive design solutions compared to the most common 2R serial kinematic chain. To increase transparency, force sensors should be mounted as close as possible to the physical interface with the user. Although non collocated actuation and force sensing make the passivity constraint more challenging to achieve [7], thus threatening coupled stability, recent developments tended to loosen this constraint to improve dynamic performances [5], [8], thus allowing the device to be unstable in isolation, but stable when coupled with the human body.

In this paper, we investigated how the burden of the exoskeleton inertia on the wearer can be reduced by measuring the interaction forces/torques at the interfaces between the robot and the user's leg, and by using these signals to close a feedback loop on the joint actuators, as opposed to closing the loop on the torque sensors mounted between the actuators and the robot links (traditional configuration). Two zero impedance controllers - one based on interaction-sensing and the other based on joint-torques - were implemented in the same unilateral exoskeleton [9], and their effect on the user's gait were assessed by experimental tests on healthy subjects. Our working hypothesis was that, by controlling the interaction error, the effects of inertial components on the user's gait would be alleviated and this, in turn, would reduce the alterations on subjects' natural gait induced by the robot.

II. Methods

A. Experimental setup

The device used in this study is ALEX II [9], a treadmill-based exoskeleton for the lower-limbs with two active DOFs

D. Zanotto is with the Dept. of Mechanical Engineering, University of Delaware, Newark, DE 19716, USA.

T. Lenzi is with the Center for Bionic Medicine, Rehabilitation Institute of Chicago, Chicago, IL 60611, USA.

P. Stegall and S. K. Agrawal (sunil.agrawal@columbia.edu) are with the Dept. of Mechanical Engineering, Columbia University, NY 10027, USA.

978-1-4673-6024-1/13/$31.00 ©2013 IEEE

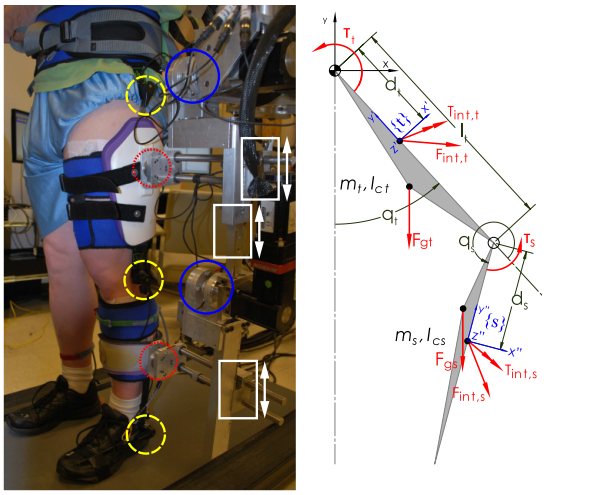

Fig. 1. Sensors and leg adjustments: torque sensors in solid blue, F/T sensors in dotted red, goniometers in dashed yellow, manual adjustments d_t, l_t and d_s in solid white (left). Kinematic scheme of the robotic leg (right).

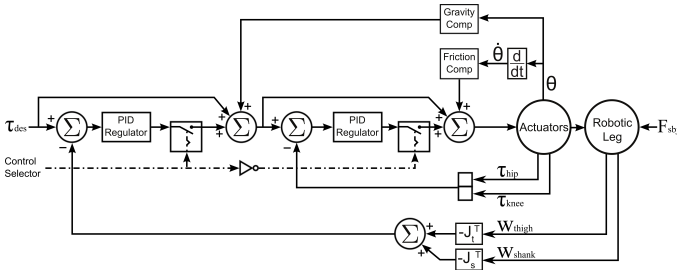

Fig. 2. Low level controllers.

at the leg (hip and knee flexion/extension) and 4 passive DOFs at the trunk (vertical rotation and anterior/posterior, superior/inferior and lateral motions). The passive DOFs can be optionally locked to restrict some of the movements of the wearer. The control architecture is based on a high level controller and a low level controller. The former allows the therapist to set a force field (either divergent or convergent) around a target footpath, which will in turn generate assistive or resistive forces on the user's foot. Based on the interaction force computed by the high level controller, corresponding torque commands are sent to the low level force controller, which is responsible for accurate tracking of the these commands. In the experimental sessions described in the following, all the passive DOFs were locked, except the anterior/posterior and the superior/inferior trunk motions. In addition to the two torque sensors (TRS Series, Transducers Techniques, Temecula, CA, USA) placed between the output shaft of each motor and the corresponding robotic link, two non collocated force/torques sensors (mini45 F/T Sensor, ATI Industrial Automation, Apex, NC, USA) were mounted at the interfaces between each link and the corresponding semi-rigid robotic orthosis (Fig. 1). For the purposes of this study, we will focus on the low level control - assuming that the desired interaction force is null - and we will compare the performances of two force-feedback controllers, one closing the loop on the collocated sensors, the other one closing the loop on the non collocated sensors.

Let us consider the model of a planar RR manipulator shown in Fig. 1. The equations of motion can be readily obtained in the form:

$$\boldsymbol{\tau}_{\mathrm{m}} = M(\mathbf{q})\,\ddot{\mathbf{q}} + V(\mathbf{q},\dot{\mathbf{q}}) + G(\mathbf{q}) + F(\mathbf{q},\dot{\mathbf{q}}) + \boldsymbol{\tau}_{\mathrm{int}}, \tag{1}$$

$\mathbf{q} = \{q_t, q_s\}^T$ is the vector of the generalized coordinates, $M(\mathbf{q}) \in \mathbb{R}^{2\times 2}$ is the position-dependent mass matrix, $V(\mathbf{q},\dot{\mathbf{q}}) \in \mathbb{R}^{2\times 1}$ is the vector of Coriolis and centrifugal terms, $G(\mathbf{q}) \in \mathbb{R}^{2\times 1}$ is the vector of gravity terms, $F(\mathbf{q},\dot{\mathbf{q}}) \in \mathbb{R}^{2\times 1}$ accounts for Coulomb and viscous friction and $\boldsymbol{\tau}_{\mathrm{int}} \in \mathbb{R}^{2\times 1}$ represents the human-robot interaction torques reflected at the joints of the manipulator. In (1), we adopted a human-centered convention for assigning the sign of $\boldsymbol{\tau}_{\mathrm{int}}$: a positive hip interaction torque indicates a torque exerted by the robot on the human hip, which tends to flex the hip. Interaction wrenches are sensed at two interfaces with the human leg, the thigh and the shank orthoses. Differential kinematics can be utilized to calculate $\boldsymbol{\tau}_{\mathrm{int}}$ based on data measured by the two force/torque sensors. Since only forces and moments acting on the plane of motion (i.e., the sagittal plane) generate torques at the knee and hip joints, the following reduced formulation is obtained:

$$\boldsymbol{\tau}_{\mathrm{int}} = -J_t^T \begin{Bmatrix} F_{x\,\mathrm{int},t} \\ F_{y\,\mathrm{int},t} \\ \tau_{z\,\mathrm{int},t} \end{Bmatrix} - J_s^T \begin{Bmatrix} F_{x\,\mathrm{int},s} \\ F_{y\,\mathrm{int},s} \\ \tau_{z\,\mathrm{int},s} \end{Bmatrix}, \tag{2}$$

where $\{F_{x\,\mathrm{int},*},\ F_{y\,\mathrm{int},*},\ \tau_{z\,\mathrm{int},*}\}^T \in \mathbb{R}^{3\times 1}$ are force/torques measured at the the thigh or shank sensors and $J_* \in \mathbb{R}^{3\times 2}$ are the corresponding Jacobian matrices:

$$J_t = \begin{bmatrix} d_t & 0 \\ 0 & 0 \\ 1 & 0 \end{bmatrix}; \quad J_s = \begin{bmatrix} d_s + l_t\cos q_s & d_s \\ -l_t \sin q_s & 0 \\ 1 & 1 \end{bmatrix}; \tag{3}$$

Notice that vectors and matrices have been written in the local frames $\{t\}$ or $\{s\}$ shown in Fig. 1. In (1), $\boldsymbol{\tau}_{\mathrm{m}} \in \mathbb{R}^{2\times 1}$ is the vector of the driving torques output by the motors, which can be though of as the sum of two contributes: the first one required to overcome actuators inertial and frictional torques (we assume friction to be mostly due to the gearboxes and negligible elsewhere), and the second one, $\boldsymbol{\tau}$, required to move the robotic leg. Equation (1) can thus be rewritten as:

$$\boldsymbol{\tau}_{\mathrm{m}} = M_{\mathrm{m}}\ddot{\mathbf{q}} + F(\mathbf{q},\dot{\mathbf{q}}) + \boldsymbol{\tau} \tag{4a}$$

$$\boldsymbol{\tau} = M_{\mathrm{r}}(\mathbf{q})\,\ddot{\mathbf{q}} + V(\mathbf{q},\dot{\mathbf{q}}) + G(\mathbf{q}) + \boldsymbol{\tau}_{\mathrm{int}}, \tag{4b}$$

where M_{m}, $M_{\mathrm{r}}(\mathbf{q}) \in \mathbb{R}^{2\times 2}$ are the mass matrices of the actuators and of the robotic leg, respectively. Figure 2 shows a scheme of the low-level force controller: it consists of a force-feedback loop and feed-forward terms to compensate gravity and friction. The commanded torque is:

$$\boldsymbol{\tau}_{\mathrm{m}} = \boldsymbol{\tau}_{\mathrm{fb}} + G(\mathbf{q}) + F(\mathbf{q},\dot{\mathbf{q}}) \tag{5}$$

The feedback loop can be closed either on the torque sensors at the gearboxes output shafts (*Torque Sensor mode*, TS in the following) or on the force/torque sensors at the robot thigh and shank orthoses (*Force/Torque Sensor mode*, FTS in the following). Based on the locations of the torque sensors (Fig. 1), we assume that their outputs are good estimations of $\boldsymbol{\tau}$: if the robot is controlled in TS mode, the regulator seeks to drive to zero the error $(G(\mathbf{q}) - \tau) = \boldsymbol{\varepsilon}_{\mathrm{TS}}$. In practice, due to limitation of the controller (e.g., limited bandwidth, errors in the gravity and friction models, etc.), this cancellation is only partial, i.e., $\|\boldsymbol{\varepsilon}_{\mathrm{TS}}\| > 0$. Plugging (5) into (4a) and then using the latter expression yields:

$$\tau_{\mathrm{fb,TS}} = M_{\mathrm{m}}\ddot{\mathbf{q}} - \boldsymbol{\varepsilon}_{\mathrm{TS}}, \tag{6}$$

whereas from (4b) we obtain:

$$\boldsymbol{\tau}_{\text{int,TS}} = -\left(M_{\text{r}}\left(\mathbf{q}\right)\ddot{\mathbf{q}} + V\left(\mathbf{q},\dot{\mathbf{q}}\right)\right) - \boldsymbol{\varepsilon}_{\text{TS}} \tag{7}$$

The former expressions indicate that, even under ideal conditions, the standard close-loop force feedback (i.e., one where actuators and force sensors are collocated) only masks a fraction of the inertial contributions of the exoskeleton (namely, those due to the rotation of the motors and gearboxes shafts), and the user is actually in charge to support the dynamical loads arising from the robotic leg moving along a certain trajectory $(\mathbf{q},\dot{\mathbf{q}},\ddot{\mathbf{q}})$. This directly affects the transparency of the device controlled in zero-force mode, and would eventually bias the assistive/resistive forces exerted on the subjects' leg when the force field control is active. Conversely, when the robot is operated in FTS mode, the regulator seeks to zero the error $\left(-\tau_{\text{int,FTS}}\right) = \boldsymbol{\varepsilon}_{\text{FTS}}$, so that interaction torques are only due to a non-ideal behavior of the controller[1]. Plugging (5) into (1) yields:

$$\boldsymbol{\tau}_{\text{fb,FTS}} = M\left(\mathbf{q}\right)\ddot{\mathbf{q}} + V\left(\mathbf{q},\dot{\mathbf{q}}\right) - \boldsymbol{\varepsilon}_{\text{FTS}}, \tag{8}$$

which shows that the FTS feedback contribution - under ideal conditions - matches the dynamic torques arising from the actuators *and* from the robotic leg.

In the following sections, we report experimental results aimed to compare the effects of the two controllers on the natural gait pattern of the wearer.

B. Experimental Protocol

Three healthy young males (age 28 ± 1 years, height 1.75 ± 0.03m, weight 72.33 ± 3.06kg) volunteered for the experiment, which consisted of 4 walking sessions, each lasting 10 minutes. Treadmill speed was set to 2.4MPH (1.1m/s) and maintained across all sessions. In the first session (baseline or BL) subjects walked on the treadmill without the robot. In the second and third sessions, subjects walked on the treadmill while their non-dominant leg (i.e., the left leg for all the subjects) was attached to the robot, which was controlled in FTS mode and TS mode, respectively. The forth session (post-test or PT) was similar to the first one. Participants were not informed about the controllers and they were instructed to walk naturally. Breaks were given between consecutive sessions (2 to 5 minutes, depending on the subject). Though lightweight, robot orthoses have a mass (medium thigh cuff: 654g, medium shank cuff: 310g) whose effect cannot be compensated by either feedback loops due to sensors locations. To assess potential effects of the robotic orthoses on natural walking, baseline and post-test sessions were split into two 5-minute-long intervals (BL was followed by BLC, PTC was followed by PT, with the additional suffix indicating that the robotic cuffs were attached to the left leg). Donning and doffing the two orthoses required less than 1 minute. The experiment was approved by the IRB of the University of Delaware, and all subjects signed an informed consent prior to the beginning of the experimental protocol. EMG signals were recorded from Tibialis Anterior (TA), Gastrocnemius Medialis (GM) and Rectus Femoris (RF) to measure the muscle activations. Sensor location and skin preparation were performed according to the SENIAM guidelines [10]. Potentiometric goniometers (PASCO, Roseville, CA) were aligned to subject's hip, knee and ankle joints by means of Velcro straps (Fig. 1). All position and force transducers were zeroed at the beginning of each session. Kinematic, kinetic and electromyographic data were sampled at 1kHz, and data collected during the last 60 seconds of each session were analyzed. Integrated EMG (iEMG) were computed after splitting the filtered and rectified signals into gait cycles (2^{nd} order band-pass Butterworth, 20-500Hz). A smoothening filter (2^{nd} order low-pass Butterworth, 4Hz) was applied to obtain the EMG Linear Envelopes (LE). Kinematic and electromyographic data were normalized based on the peak values measured in the BL session. Average results on scalar metrics are reported in the bar-plots, whereas trends over the gait cycle are reported from one representative subject.

[1]Notice, however, that the vector $\boldsymbol{\tau}_{\text{int}}$ does not *exactly* estimate the equivalent torques felt by the user: (i) misalignments between human and robot joints are not considered in the model; (ii) there are inertial components arising from the orthoses which cannot be zeroed due to the location of the F/T sensors.

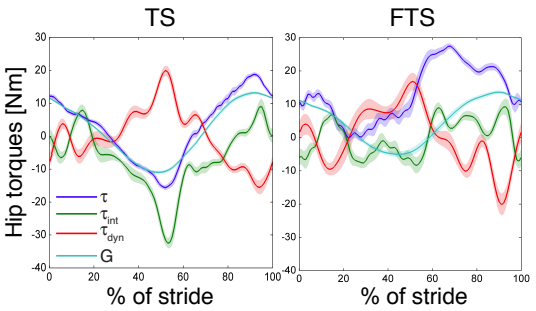

Fig. 3. Individual contributes to the hip joint torque for the TS and FTS controllers. Shaded areas indicate ±SD

III. Results

A. Model Validation

Figure 3 illustrates the contributions of the torques mentioned in Section II-A at the hip joint, as a subject walked in the robot, while the latter was controlled either in TS mode or in the FTS mode. $\boldsymbol{\tau}$, $\boldsymbol{\tau}_{\text{int}}$ and $G\left(\mathbf{q}\right)$ were computed in real-time and stored in the controller[2], whereas the dynamics contributions $\boldsymbol{\tau}_{\text{dyn}}$ where estimated off-line, based on the nominal mass properties of the robotic leg and on acceleration data derived by double-differentiating and filtering the encoder readings (Butterworth 4th order, $f_c = 4$Hz). Experimental data are consistent with (7), the trends of $\boldsymbol{\tau}_{\text{int}}$ and $\boldsymbol{\tau}_{\text{dyn}}$ being almost symmetric in TS mode. $\boldsymbol{\tau}$ approximately tracks $G\left(\mathbf{q}\right)$ except when the thigh reverses the direction of movement, thus increasing the contribute due to actuator dynamics. Additionally, one can notice that $\boldsymbol{\tau}_{\text{dyn}}$ and $G\left(\mathbf{q}\right)$ follow opposite trends, their magnitude being comparable. This fact has at least two implications on the design of robotic exoskeletons for the lower limbs: (i) in terms of transparency, masking inertia of the links might be as important as compensating for gravity, even though the latter is much easier to implement; (ii) gravitational and inertial terms of the robot links partially balance each other, so that removing gravity compensation in TS mode might actually reduce $\boldsymbol{\tau}_{\text{int}}$. Indeed, the regulator would seek

[2]Error propagation was applied to check that measured wrenches could be mapped to joint torques with sufficient accuracy. We assumed 2.5mm as the worst-case uncertainty on each leg adjustment d_t, d_s, l_t and neglected other sources of misalignments. Uncertainties on force/torque measurements were retrieved from calibration certificates. Based on these inputs, the analysis yielded: $\Delta\boldsymbol{\tau}_{\text{HIP}} = \pm 0.5$Nm, $\Delta\boldsymbol{\tau}_{\text{KNEE}} = \pm 0.15$Nm.

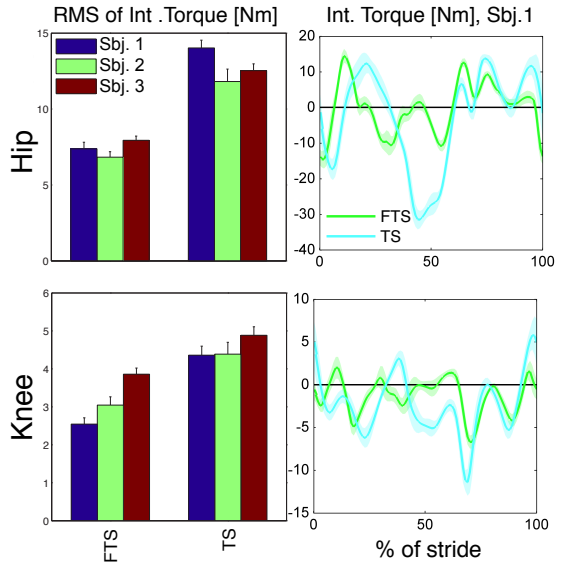

Fig. 4. RMS interaction torques and average interaction torques over the gait cycle for a representative subject (shaded areas and error bars represent ±SD).

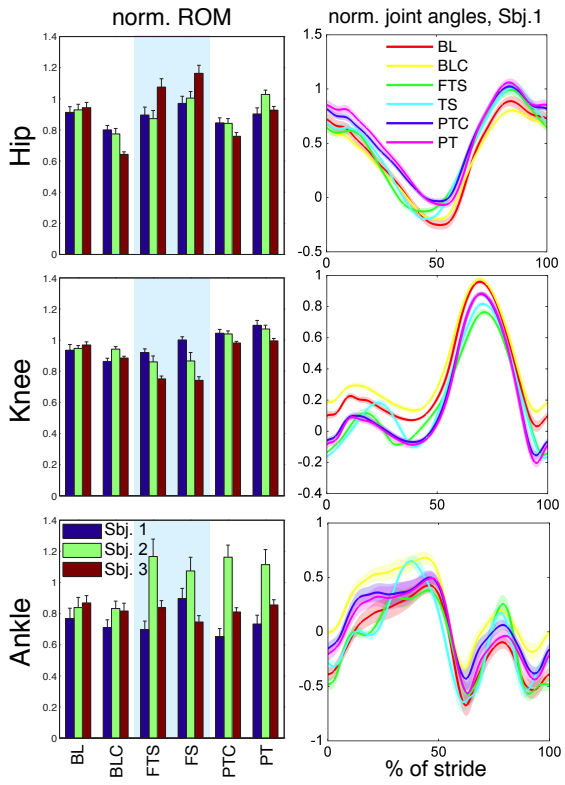

Fig. 5. Normalized ROM and averaged normalized joint angle for a representative subject (shaded areas and error bars represent ±SD).

to zero $(-\boldsymbol{\tau}) = \boldsymbol{\varepsilon}'_{\mathrm{TS}}$, thus if the balance was perfect (as in a pendulum), (4b) would yield $(-\tau_{\mathrm{int,TS}}) = \boldsymbol{\varepsilon}'_{\mathrm{TS}}$, similarly to the FTS mode. A drawback of this approach compared to FTS mode, however, is that the quality of the canceling depends on gait cadence and on the mass distribution of the robotic leg [11]. When the FTS mode is active, the driving torque at the hip joint approximately compensates for gravity, friction and inertia of the robot. The effect is a general reduction of the hip interaction torques with respect to the TS controller (Fig. 3).

B. Interaction Torques

Figure 4, left side, shows the average RMS value of $\boldsymbol{\tau}_{\mathrm{int}}$ over sessions FTS and TS: the FTS controller effectively reduced the RMS of the hip interaction torque and, to a less extent, also the knee interaction torque ($\boldsymbol{\tau}_H$ -42.1%, $\boldsymbol{\tau}_K$ -31.1% on average). Torque profiles over the gait cycle (GC) show that peak values were reduced even further (Fig. 4, right side). The less evident effects measured at the knee joint can be explained with the moment of inertia of the shank link about the knee joint being smaller than the overall moment of inertia of the robotic leg reflected at the hip joint. The highest interaction torques were detected at the inversion of movement. A peak negative hip torque at $\approx$ 45%GC was measured, corresponding to the thigh suddenly inverting the direction of movement as it started flexing to get ready for the swing motion (Fig. 5). In this phase, the extending robotic thigh must be decelerated first, and then accelerated in the opposite direction. The moment of inertia of the serial robotic structure about the hip joint is large at this time, the shank being approximately aligned with the thigh. With the TS controller, this dynamic torque is mostly provided by the user's leg, thereby the user's torque input is significantly larger than it is for the FTS controller (-95.3%). At mid swing ($\approx$ 70%GC) a negative peak in the knee torque was measured, which corresponds to the point of maximum knee flexion, after which the knee starts extending to prepare the leg for the next heel strike. Again, the inversion of motion of the robot shank link requires certain dynamic torques that had to be entirely provided by the subject in the case of TS controller. The FTS controller reduces the torque input in this condition by -46.6%. A third torque peak was found in the knee before the heel strike ($\approx$ 97%GC), when the knee slight flexes to favor shock absorption. Even in this case, the torque reduction was evident (-73.5%). Interaction torques for the FTS controller were not null due to non compensated effects of control, yet they were substantially reduced within ±10Nm and ±5Nm for hip and knee joints, respectively. Even though these results are in line with current treadmill-based exoskeletons, they still represent a significant fraction of the equivalent torques applied by human muscles at the hip, knee and ankle joints in normal walking [12]. Thus, even though the FTS controller showed better performance than the TS controller, still the contribute of the robot to the gait cycle was not negligible.

C. Gait kinematics

Figure 5, left side, shows the average normalized range of motion (ROM) for the hip, knee and ankle joints over all the sessions. Walking with thigh and shank orthoses reduced hip, knee and ankle ROM. Reductions were - in general - slightly higher for the difference BL-BLC than they were for PT-PTC. Results for ankle were relatively small (BL-BLC: -4.7%, PT-PTC: -4.0%, less than 2deg on average). Larger differences were measured at the knee (BL-BLC: -5.6%, PT-PTC: -3.0%, less than 4 deg on average), and at the hip (BL-BLC: -20.2%, PT-PTC: -14.2%, less than 7 deg on average). These results confirm previous findings [13], [14], which suggest that loads $<$ 2kg attached to the lower

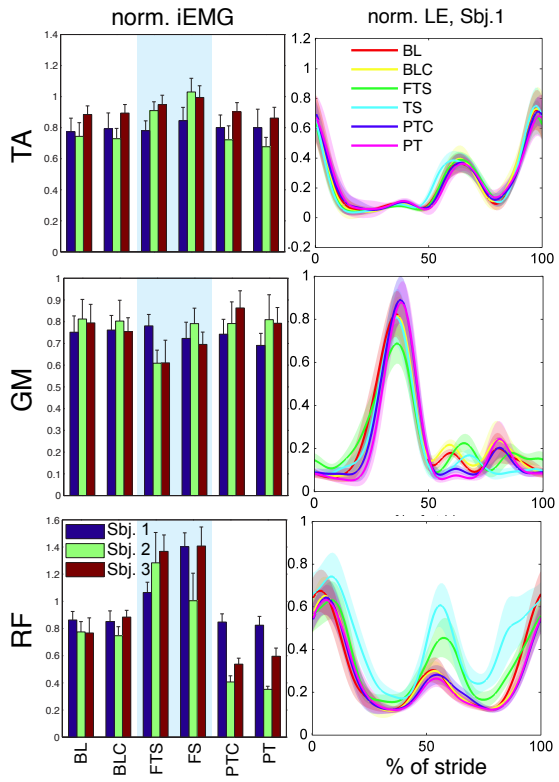

Fig. 6. Normalized iEMG and averaged normalized EMG Linear Envelope for a representative subject (shaded areas and error bars represent ±SD).

extremities can alter gait kinematics significantly.

Walking in the robot increased the hip ROM, the results being more marked and consistent among the subjects for the TS controller (FTS $+2.0\%$, TS $+12.6\%$ on average). The ankle ROM also increased more in the TS control mode (FTS $+8.8\%$, TS $+10.3\%$), but results were mixed. The knee ROM was affected in the opposite way, with larger decreases measured in the FTS controller (FTS -11.8%, TS -8.3%). A closer look at the hip angle over the gait cycle in the 3 subjects revealed that - in general - the increments were due to larger extension peaks in late stance. In this phase, the inertia of the links is actually applying a negative torque on the extending hip joint (Fig. 4, TS controller), which tends to extend the hip further, thus delaying the inversion of motion. The interaction torque was smaller for the FTS mode in this phase, thus explaining the reduced effects on the hip kinematics. Reductions on knee ROM were mainly due to a smaller flexion peak in the mid swing. Prior to the flexion peak ($\approx 70\%$GC), the lower leg is flexing and the interaction torque is negative: the power flow from the robot to the human leg is therefore positive, indicating that the robot is actually favoring the flexion movement. The decelerating (resistive) torque was provided by the RF, whose activation actually increased while walking in the robot. Therefore, the decrease in the amount of flexion might be due to the RF over-compensating for the action of the robot.

D. Muscle activations

Muscle activity of TA, GM and RF were negligibly affected by the orthoses (Fig. 6). Increased efforts were measured in the TA in sessions FTS and TS, the deviations from BL being larger for the latter control mode (FTS $+10.1\%$, TS $+20.0\%$). Inspection of the individual linear envelope profiles showed that increments were due to two reasons: slightly early commencement of the secondary burst (foot clearance), and increased peak activity at heel strike (plantar-flexion moment to counteract ground reaction forces). The former effect, together with the results obtained on gait symmetry, indicates that subjects' weight was mostly supported by the free leg when they wore the exoskeleton. The latter effect, quantitatively less evident, might be caused by increased plantar-flexing moments produced by ground reaction forces at heel strike. These increments, due to the inertia of the links, required larger efforts by the TA to control the rate of foot plantar-flexion (i.e., avoid foot slap).

Similarly, activation of RF increased when walking in the robot, the effects being - in general - more evident for the TS controller (FTS $+55.8\%$, TS $+58.6\%$), even though subject 2 showed an opposite trend. Visual inspection determined that increments were most apparent in the second burst of activation ($\approx 60\%$GC), which is responsible for swinging the upper leg forward (hip flexor) and decelerating the flexing lower leg (knee extensor). In this phase, the robot is actually helping hip flexion but resisting the deceleration of the lower leg (Fig. 4), its action being larger for the TS controller. Thus, the increased activity in RF might be related to increased efforts in decelerating the lower leg due to the robot, and the FTS controller partially alleviated this effect. RF activations tended to decrease below the baseline values in the post tests, allowing the knee to flex slightly more than in the BL session, as indicated by larger knee ROM (Fig. 5). This might be an aftereffect, even though one would expect an aftereffect to decrease knee flexion instead of increasing it. An alternative hypothesis for the drop-off in the RF activations shown by subjects 2 and 3 in the post-tests is poor electrode connectivity due to sweating, which might have affected EMG readings. The Velcro straps and the robot orthoses covering the electrodes might have contributed to increased sweating in this region due to lack of breathability.

Small decrements in the activation of the GM were measured in FTS and TS sessions, the difference being more evident for the FTS controller (FTS -14.8%, TS -6.3%). Reductions were found mainly in the major burst of the muscle, when the GM acts as a foot plantar-flexor to provide the push-off force that propels walking. While walking, the human body (legs, head, arms and trunk) forms a complex dynamic system. It is therefore not surprising that applying external forces at the hip and knee joints would affect the overall dynamics of the system, eventually inducing motor adaptation at the ankle, even though the latter was not directly connected to the robot. Several studies provided evidences for the existence of two concurring/interchanging walking strategies for gait propulsion: ankle-strategy and hip-strategy [15], [16], with healthy gait being a trade-off between the two, and the ankle-strategy being predominant for healthy young adults [17]. Transitioning from the ankle to the hip strategy reduces plantar-flexing moment [15], the converse effect having also been observed [17]. The interaction torques measured in this experiment act as disturbances on the human motor control system, which adapts to the modified dynamic conditions. Thus, the concurrent increase in RF activity and decrease in GM activity measured in FTS and TS suggest a

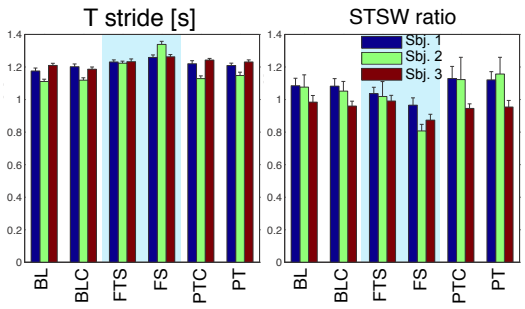

Fig. 7. Average stride period and average stance-to-swing ratio (*STSW ratio*, left leg over right leg).

change in walking strategy from ankle-strategy to hip-strategy due to the interaction with the robot.

E. Gait timing

Walking in the robot increased the mean stride period (Fig. 7), the deviations being more evident when the robot was controlled in TS mode (FTS $+5.6\%$, TS $+10.7\%$), presumably because the former was more effective in masking the link inertia. It has been reported that increasing the moment of inertia of the legs by adding weights induces larger stride period and swing time [13], and similar results have been obtained when the additional inertial loads were generated by a robotic leg [5]. Since the walking speed was fixed, the reduction in cadence corresponded to proportionally longer stride length, which was correlated to the increased hip ROM discussed above. STSW ratio is the ratio between the stance to swing of the left leg (attached to the robot) and that of the right leg. Walking in the robot negatively affected symmetry, the effect being more evident for the TS controller (FTS -3.0%, TS -15.7%). Results indicate that, when walking in the robot, subjects's weight was mostly supported by the right leg. Several studies reported the same effect when the natural mass/inertia of the human leg was increased either by additional loads [14], [18] or by a robotic exoskeleton [19]–[21].

IV. Conclusion

In this study, we showed that a force-feedback controller which utilizes the interaction forces/torques between the robot and the user's leg as feedback signals can improve the transparency of a robotic gait trainer compared to the more commonly used force-feedback controller which exploits the feedback signal from collocated torque sensors. Although two simple zero-impedance controllers were compared in the experimental validation, those can be thought of as low-level subsystems of more complex hierarchical controllers.

Results indicated that: (i) the traditional controller lets the wearer carry the inertial loads generated by the robot links; (ii) the interaction-sensing-based controller substantially reduced the interaction torques, thereby inducing smaller changes in the user's natural gait in terms of hip ROM, gait timing, gait symmetry and activations of the TA and RF muscles. This approach can be used to improve the transparency of existing devices with minimal redesign efforts (compact 6-axes load cells can be placed at the pre-existent interfaces between the robotic links and the orthoses worn by the user) and a relatively small increase in the total cost of the robot (multiple-axes sensors are, in general, more expensive than single axis load-cells).

References

[1] E. Wolbrecht *et al.*, "Optimizing compliant, model-based robotic assistance to promote neurorehabilitation," *IEEE Trans Neural Syst Rehabil Eng*, vol. 16, no. 3, pp. 286–297, 2008.

[2] S. K. Banala *et al.*, "Robot assisted gait training with active leg exoskeleton (alex)." *IEEE Trans Neural Syst Rehabil Eng*, vol. 17, no. 1, pp. 2–8, Feb. 2009.

[3] J. F. Veneman *et al.*, "Design and evaluation of the LOPES exoskeleton robot for interactive gait rehabilitation," *IEEE Trans Neural Syst Rehabil Eng*, vol. 15, no. 3, pp. 379–386, 2007.

[4] K. Kong *et al.*, "A cable-driven human assistive system and its impedance compensation by sensor fusion," in *Proc. of the ASME Dynamic Systems and Control Conference, DSCC'10*, 2010.

[5] G. Aguirre-Ollinger *et al.*, "Design of an active one-degree-of-freedom lower-limb exoskeleton with inertia compensation," *Int J Robot Res*, vol. 30, no. 4, pp. 486–499, 2011.

[6] D. Zanotto *et al.*, "ALEX III: A novel robotic platform for gait training - design of the 4-dof leg," in *Proc. of the IEEE Int. Conf. on Robotics and Automation, ICRA'13*, Karlsruhe, Germany, May 6-10 2013.

[7] E. Colgate *et al.*, "An analysis of contact instability in terms of passive physical equivalents," in *Proc. of the IEEE Int. Conf. on Robotics and Automation, ICRA'89.*, 1989, pp. 404–409.

[8] S. Buerger *et al.*, "Relaxing passivity for human-robot interaction," in *Proc. of the IEEE/RSJ Int. Conf. on Intelligent Robots and Systems, IROS'06*, 2006, pp. 4570–4575.

[9] K. N. Winfree *et al.*, "Design of a minimally constraining, passively supported gait training exoskeleton: ALEX II," in *Proc. of the IEEE Int. Conf. on Rehabilitation Robotics, ICORR'11*, 2011, pp. 1–6.

[10] H. Hermens *et al.*, *European recommendations for surface electromyography*. Roessingh Research and Development The Netherlands, 1999.

[11] H. Vallery *et al.*, "Optimized passive dynamics improve transparency of haptic devices," in *Proc. of the IEEE Int. Conf. on Robotics and Automation, ICRA'09.*, 2009, pp. 301–306.

[12] D. A. Winter, *The biomechanics and motor control of human gait: normal, elderly and pathological*. Univarsity of Waterloo Press, 1991.

[13] T. Royer *et al.*, "Manipulations of leg mass and moment of inertia: effects on energy cost of walking." *Med Sci Sport Exer*, vol. 37, no. 4, p. 649, 2005.

[14] J. Noble *et al.*, "Adaptation to unilateral change in lower limb mechanical properties during human walking," *Exp Brain Res*, vol. 169, no. 4, pp. 482–495, 2006.

[15] M. Mueller *et al.*, "Hip and ankle walking strategies: effect on peak plantar pressures and implications for neuropathic ulceration." *Arch Phys Med Rehab*, vol. 75, no. 11, p. 1196, 1994.

[16] T. Lenzi *et al.*, "Powered hip exoskeletons can reduce the user's hip and ankle muscle activations during walking," *IEEE Trans Neural Syst Rehabil Eng*, vol. in press, 2013.

[17] C. Lewis *et al.*, "Walking with increased ankle pushoff decreases hip muscle moments," *J Biomech*, vol. 41, no. 10, pp. 2082–2089, 2008.

[18] H. Skinner *et al.*, "Ankle weighting effect on gait in able-bodied adults." *Arch Phys Med Rehab*, vol. 71, no. 2, p. 112, 1990.

[19] E. Van Asseldonk *et al.*, "The effects on kinematics and muscle activity of walking in a robotic gait trainer during zero-force control," *IEEE Trans Neural Syst Rehabil Eng*, vol. 16, no. 4, pp. 360–370, 2008.

[20] J. Kim *et al.*, "Visual and kinesthetic locomotor imagery training integrated with auditory step rhythm for walking performance of patients with chronic stroke," *Clin Rehabil*, vol. 25, no. 2, pp. 134–145, 2011.

[21] D. Zanotto *et al.*, "Effects of complementary auditory feedback in robot-assisted lower extremity motor adaptation," *IEEE Trans Neural Syst Rehabil Eng*, vol. in press, 2013.